COBEM 2021 26th International Congress of Mechanical Engineering
ABCM Associação Brasileira de Engenharia e Ciências Mecânicas
November 22-26, 2021, Virtual Congress, Brazil

COB-2021-1934
AERODYNAMIC AND ACOUSTIC CHARACTERIZATION OF PROPELLER VIA A LATTICE-BOLTZMANN BASED LES

Mateus Grassano Lattari
Victor Henrique Pereira da Rosa
mateus.grassano@polo.ufsc.br, victor.rosa@polo.ufsc.br
César José Deschamps
Universidade Federal de Santa Catarina
Deschmaps@polo.ufsc.br

Abstract. *Recent designs of electrical aircraft are the main driver for new applications of propellers in civil aviation, such as delivery UAVs, urban transport, eVTOLs, and small-scale regional electrical aircraft. As expected, these new applications imply propeller-powered aircraft operating in highly populated urban areas, making the resulting noise a critical design issue. In this paper, a numerical method consisting of a lattice-Boltzmann-based Large Eddy Simulation approach is assessed to predict the aerodynamics and noise of isolated propellers. Numerical results are presented for thrust, torque, and power-spectral density in the far-field. Comparison with measurements available in the literature shows that the method can predict the aerodynamic parameters and 1st-BPF tones within 10% and 5dB of the experimental data, with a fraction of the computational processing cost of traditional LES approaches.*

Keywords: *propeller simulation,LBM, PowerFLOW, Aeroacoustics, CFD.*

1. INTRODUCTION

Recent advances in electric batteries allow a wide range of new applications in the transport industry, as vehicles could be powered by electrical engines. Regarding the aerospace industry, these engines could enable new possibilities of usage for propeller-powered aircraft. These possibilities arise from known limitations of combustion engines, such as the impossibility of providing high torque rates in low rotational speeds, altitude dependence of combustion performance, and high maintenance demands compared to the electrical engines. Moreover, the emissions of combustion engines are one of the main issues in the environmental impact of the aviation industry, which could be majorly attenuated by the electrical ones.

Although electrical engines seem promising, they still face major disadvantages against combustion engines. The most critical one is related to its battery's energy density, which is more than ten times smaller than fossil fuels (Rohacs and Rohacs, 2019). This has serious implications for the aircraft's weight and autonomy. As a result, these battery limitations still majorly limit aircraft electrification to propeller-driven small ones. On the other hand, the limitation opens a branch of new types of aircraft such as UAV, eVTOL, and small passenger airplanes that could operate in urban delivery systems, air taxis, and short-range flights (Viswanathan et al., 2019; Airway, 2020; Castillho, 2020), and demonstrated in Figure **??**. While those new airplanes could provide new behaviors, their possible proximity with highly populated areas could generate too much noise. As aircraft noise is highly regulated (Smith, 2004), especially in cities, a rigorous propeller aerodynamic and acoustic assessment is mandatory.

(a) UAV (b) eVTOL

Figure 1: UAV and EVTOL implementations. Adapted from Airway (2020) and Castilho (2020)

As so, one of the key aspects of propeller design involves the predictions of its aerodynamic performance and its noise emissions. The aerodynamic performance can be predicted using the implementation of well-established low-order models such as the Blade Element Momentum Theory or the Vortex lattice Method (Strash et al. 1998; Ol et al., 2008; Leng et al., 2019; Igraham et al., 2019) On the other hand, the same strategy is not similar regarding its acoustic behavior, as the acoustic phenomena are much more complex.

The reasons for these complexities arise from the nature of the propeller noise, resulting in a very characteristic noise spectrum. It is dominated by two types of noise: broadband and tonal noise. The tonal noise corresponds to the noise generated because of periodic passage of the propeller blade, so that the spectrum is marked with high energy in each Blade Passing Frequency - BPF. The broadband represents small peaks of energy oscillations widely distributed in a wide range of frequencies in the spectrum. This behavior is a consequence of complex flow mechanisms such as instabilities waves, turbulence, and vorticities. Although the energy contributions from each broadband energy peak are much smaller than the tonal peaks, the widespread frequency bands of its energy put the broadband as a significant part of the propeller noise.

Regarding models to predict the noise, the tonal type can be well predicted in low order flow models and analogies, such as the one by Amiet and Roger (2008). Due to its nature and complex sources, broadband noise requires complex numerical models or experiments to be evaluated. Experiments can permit a better understanding of those phenomena, but in the early conception stages, they could represent high costs or impracticalities. On the other hand, in traditional high-order computational fluid dynamics simulations, such as LES and uRANS, the noise can be predicted very accurately, and results very close to experiments can be realized. However, those models require several processing hours or difficulties in implementation that could pair them to the costs and impracticability from experiments.

Alternatively, numerical implementations of the Boltzmann Equation, the lattice-Boltzmann Method, allow results with the same error order as classic LES and uRANS implementations as reported by Gonzalez et al. (2018). Those models are modifications from traditional LES methods where the mean flow is resolved using lattice-Boltzmann and the sub mesh scale is modeled using a turbulence model. In aeroacoustics simulation of a propeller, the commercial code PowerFLOW is one of the most promising platforms for this method, as reported in recent works (Avallone et al., 2018) (Avallone et al., 2019) where its predictions account for no more than 5 dB differences in OASPL and narrow-band BPF prediction as good as 1 dB. For aerodynamic results, thrust and torque coefficients show differences from experimental results as good as 15% differences. Regarding the computational costs, the method, compared to LES, deliveries the same result with four times less the computation hour, as reported by Golzalez et al. (2018). In this work, we conduct an evaluation of PowerFLOW for the prediction of the aerodynamic performance and noise emission from a small-scale propeller. Due to the nature of this noise, this evaluation is conducted separately: evaluation of the noise spectrum from the complete signal, tonal noise, and broadband noise. The next sections present the mathematical and computational methodology performed in PowerFLOW, the results from this evaluation, and, in the end, the conclusions regarding them.

2. METHODOLOGY

2.1 Mathematical Methods

2.1.1 lattice Boltzmann based LES

Due to the impracticalness to fully simulate a system considering all its molecules in a classical mechanic's approach [1], many thermodynamics and fluid dynamics systems are modeled using a statistical mechanics one. Among these approaches, an important theoretical development is Boltzmann's one. This development associates the state of the system many particles with the transport equation of its Probability Density Function - PDF. This led to an integro-differential equation where its non-homogeneous term integrate all collision possibilities in a control volume's molecules (Krüger,2016; Succi, 2018):

$$D_t f \equiv \left[\partial_t + \frac{\vec{p}}{m}.\partial_{\vec{x}} + \vec{F}.\partial_{\vec{p}}\right] f(\vec{x},\vec{p},t) = C \tag{1}$$

where $f(\vec{x},\vec{p},t)$ is the control's volume PDF, $\vec{x},\vec{p},t$ is the particle position, momentum and temporal position,$\vec{F}$ is an external force vector, C is the integral collision term and t is the temporal dimension.

As Equation (**??**) is an integro-differential one, it still imposes several solutions difficulties, including numerical ones, because of its collision term (C). This term has such a degree of complexity as it considers all the possibilities of molecular collisions in a fluid control volume. Although many experiments have been showing that the collision could be simplified to finite effects, it was only with the advent of the model proposed by Bhartknar et al. (1954) that this equation was

[1] Classical mechanics, in this context, means the raw treatment of every molecule as a material point considering its linear momentum and position. So this would escalated to a control volume where its molecules are modeled by a minimal of two equations

majorly simplified by a collision succeed by relaxation time to an equilibrium situation:

$$C = \frac{f_o - f(\vec{x}, \vec{p}, t)}{\tau} \tag{2}$$

where f_o is the equilibrium probability density function and τ is the relaxation time. This allowed to the development of numerical implementations of Equation (**??**). The most widely used is the one called lattice-Boltzmann, in this approach the collisions are limited to finite directions and the control's volume PDF is thought to be discrete in space , where each "molecular conglomerate" is modeled by one point of the PDF. Those assumptions led to deterministic positions in the volume where each cell is connect to the adjacent one by its collisions possibilities. As a consequence, the information of each PDF is transported in the volume by this collision possibilities and this systems forms a net or lattice. This lattice is organized in its space dimensions (Dx) and the possibilities of collisions, including rest (Dy), as displayed in Figure **??**. In this present implementation, the lattice employed is the D3Q19. This model spans a transport model much simpler than Navier-Stokes equations' terms , identified as the lattice-Boltzmann equation:

$$f_i(x + c_i \triangle t, t + \triangle t) = f_i(\mathbf{x}, t) + C(\mathbf{x}, t) \tag{3}$$

where the subscription i refers to the direction of the collision in the lattice and the $\triangle$ means the discrete displacements betwen two lattice molecular conglomerates and the timesteps.

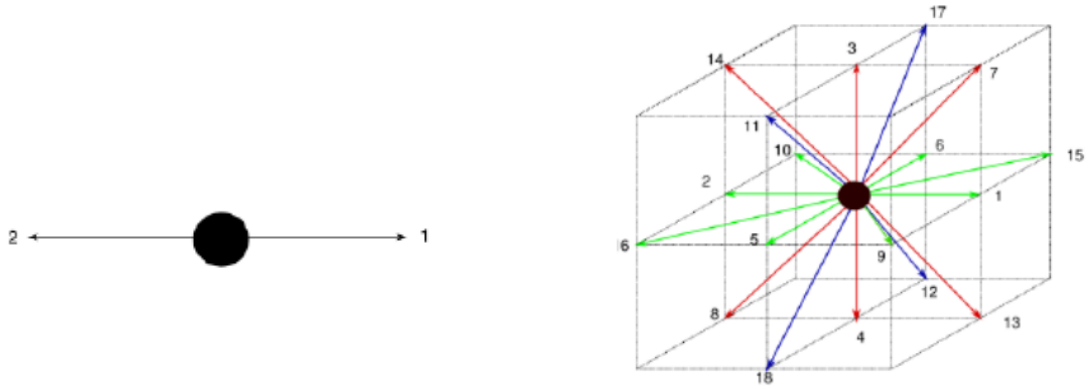

(a) D2Q3 (b) D3Q19

Figure 2: lattice classification

In PowerFLOW this model solves the mesh scale of a fluid flow and integrating it to a turbulence model, it states the foundation of the lattice Boltzmann-based LES in use for this work (Dassault, 2019). In a lattice-Boltzmann based LES the turbulence model of the submesh is integrated to the mesh scale by its effective viscosity, which is the summation of the mean flow viscosity and the turbulent viscosity. Considering the Chapman–Enskog theory the viscosity is a function of the relaxation time (SUCCI, 2018). This fact allows the definition of an effective relaxation time, which, as the viscosity, is a summation of the turbulence and mean flow relaxation time (Zhu and Carolus, 2017). The turbulence model implemented in PowerFLOW is the k-/epsilon RNG:

$$\frac{\partial}{\partial t}(\rho k) + \frac{\partial}{\partial x_i}(\rho k u_i) = \frac{\partial}{\partial x_j}\left[\left(\mu + \frac{\mu_t}{\sigma_k}\right)\frac{\partial k}{\partial x_j}\right] + P_k - \rho\epsilon \tag{4}$$

$$\frac{\partial}{\partial t}(\rho \epsilon) + \frac{\partial}{\partial x_i}(\rho \epsilon u_i) = \frac{\partial}{\partial x_j}\left[\left(\mu + \frac{\mu_t}{\sigma_\epsilon}\right)\frac{\partial \epsilon}{\partial x_j}\right] + C_{1\epsilon}\frac{\epsilon}{k}P_k - C^*_{2\epsilon\rho}\rho\frac{\epsilon^2}{k} \tag{5}$$

where μ and μ_t is, respectively, the dynamic viscosity and the turbulent dynamic viscosity, and ϵ is the turbulent dissipation and k is the turbulent kinetic energy, P_k is the production of turbulent kinetic energy, ρ is the fluid density and σ_ϵ,σ_k, $C_{1\epsilon}$ and $C^*_{2\epsilon\rho}$ are models constants.

Additionally, the model in PowerFLOW models the near-wall boundary layer using the Wall model developed by von Kármán (1931), which is represented in Figure **??** and in its most external regions of the boundary layer, the fluid velocity is governed by a log law.

Finally, PowerFLOW uses a far-field noise propagation model, as in the case of an isolated propeller free-field simulation, one can consider that all system sources are concentrated in a finite volume. This implies that all fluid outside this

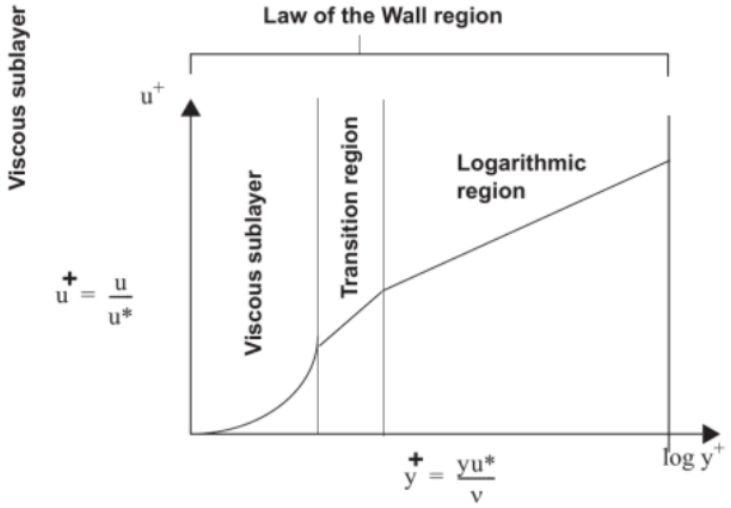

Figure 3: von Kármán Law. Adapted from Dassault (2019).

volume is at rest and in a homogenous state. This was first observed by Lighthill et al. (1951) and, following this purpose, Ffowcks Williams and Hawkings (1969) developed a theory where all sources in that volume could be described as the fluctuations of both pressure and velocity in its surface. When applying those concepts to the non-homogeneous wave equation it drives to Ffowcs Williams' equation:

$$4\pi(\rho(\mathbf{x},t)-\rho_o) = \frac{\partial^2}{\partial x_i \partial x_j}\int\left[\frac{\mathbf{T_{ij}J}}{r|1-M_r|}\right]d\eta - \frac{\partial}{\partial x_i}\int\left[\frac{p_{ij}n_jA}{r|1-M_r|}\right]dS(\eta) \tag{6}$$
$$+\frac{\partial}{\partial t}\int\left[\frac{\rho_o v_n}{r|1-M_r|}\right]dS(\eta)$$

where c is the speed of sound, is the mean density perturbation, is the Lighthill tensor (1951), F is the surface-describing function, the surface-normal velocity component, and is the Dirac delta, J is a Jacobian, r is the distance between the sources and the farfied, M_r is the wave propagation speed, η are the physical domain Lagrangian and S is the function taht defines those coordinates.

Therefore, the knowledge of the flow properties in this surface can allow that the noise can be propagated to any point in the system, which is known as the far-field. In this work, a numerical form based on Equation (**??**) is implemented, with more details about it in the next section.

2.2 Computational Methods

In PowerFLOW, such as in other standard software, the mesh is discretized in different resolution regions throughout the simulation domain. In this implementation, the refines follow sequentially circumscribe spheres regions with respect to the center of the propeller, where every interior one has more resolution than the exterior. Special treatment is given to the propeller geometry, highlighting its blade leading edge and trailing edge, as shown in Fig. 4. The results were verified for truncation error, by using three grid refinements: (i) grid 1 with 17 Million element, (ii) grid 2 with 34 Million elements (iii) grid 3 with 435 Million elements. Results of thrust and torque coefficients were found to vary by 4.52% and 4.32%, respectively, when the grid was varied from grid 1 to grid 2 and 0.68% and 0.10%, when the grid as varied from 2 to 3. Similar test for the OASPL showed deviations no more than 0.4 dB.

The simulations are conducted in different propeller rotational speed, it is considered the measurement from ten complete rotations. Those measurements are taken after six complete rotations, this allows that all domains are sensibilize by the boundary conditions and that the system leaves a transient state.

The numerical implementation of the far field model is implemented by the definition of a surface where the pressure and velocity fluctuations from then rotations are stored. This surface is defined as a cinder containing the propeller. In this work, the fluctuation from the inferior side of the cylinder are disconsidered. This enables non acoustics contributions from the propeller wake to be neglected.

As stated in the introduction, the propeller noise spectrum is formed by the overlapping of different noise types. For this reason, this study implements different signal processing techniques for each of those noise types. The complete signal is treated considering bands of frequencies from ½ BPF to 10 kHz. The choice to set a minimal frequency of ½ BPF allows that non-propeller sources, such as the motor rotation, can be excluded from the energy contribution. This

(a) Circunscreve spheres' mesh refinement. (b) Propeller's refinements.

Figure 4: Mesh refinements.

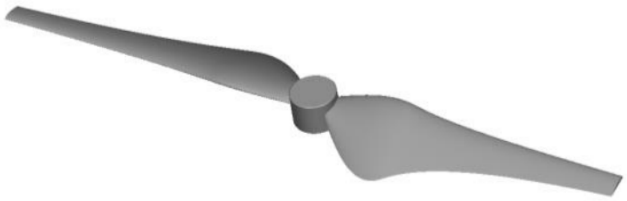

Figure 5: Reproduction of HKUST (2020) propeller.

spectrum is analyzed by its Power Density Spectrum - PSD calculated using the method developed by Welch (1967). The spectrum level in db/Hz is obtained as:

$$PSD = 10log_{10}|\frac{S_{xx}}{(2.10^{-5})^2}| \tag{7}$$

where S_{xx} is the pressure spectrum calculated via Welch's method.
By its integration its Sound Pressure Level - SPL, resulting in the Overall Acoustics Sound Pressure Level OASPL:

$$SPL[db] = PSD + 10log_{10}(\triangle f_b) \qquad OASPL[db] = 10log_{10}(\sum_{f=0kHz}^{f=10kHz} 10^{SPL(f/10)}) \tag{8}$$

where $\triangle f_b$ is the frequency band size.

Additionally, for analyzing the BPF SPL level, a narrow band filter is employed. Tests between many types of filters showed a preliminary evidence that the ensembling average one could lead to more suitable results. In this technique implementation a mean signal of one rotation, calculated from 10 rotations average, is obtained. The spectrum of this signal is dominated by propeller rotation periodic levels. This allowed a efficiency way to extract the BPF levels as high frequency bands levels are excluded and the spectrum is formed by periodic peaks with respect to the BPF multiples.

3. RESULTS

The chosen propeller's experiments for this assessment are a set of measurements conducted by HKUST (2020). The propeller has a 240 mm diameter and two blades. The set of experiments were conducted at a range of speeds of 60 to 120 Rotations Per Second - RPS in 10 RPS steps. The propeller CAD model was obtained from HKUST (2020) and then simulated in PowerFLOW with an average cost of 0.90 kCPUh, also the CAD reconstruction of the propeller is displayed in Figure 5.

3.1 Aeordynamic

Figure **??** displays the comparison between the thrust coefficient from experiments and predicted by PowerFLOW implementation. The deviations are no higher than 15% in the range of 60 to 90 RPS, after this range, the deviations drop to less than 2%. This is possibly an issue from the turbulence model implementation, as it was observed that the

turbulence intensity drops abruptly. It follows that in Figure 6 (b), deviations less than 25% are observed and, in the range after 90 RPS, they drop to 15%. This occurred for the same reason as previously stated.

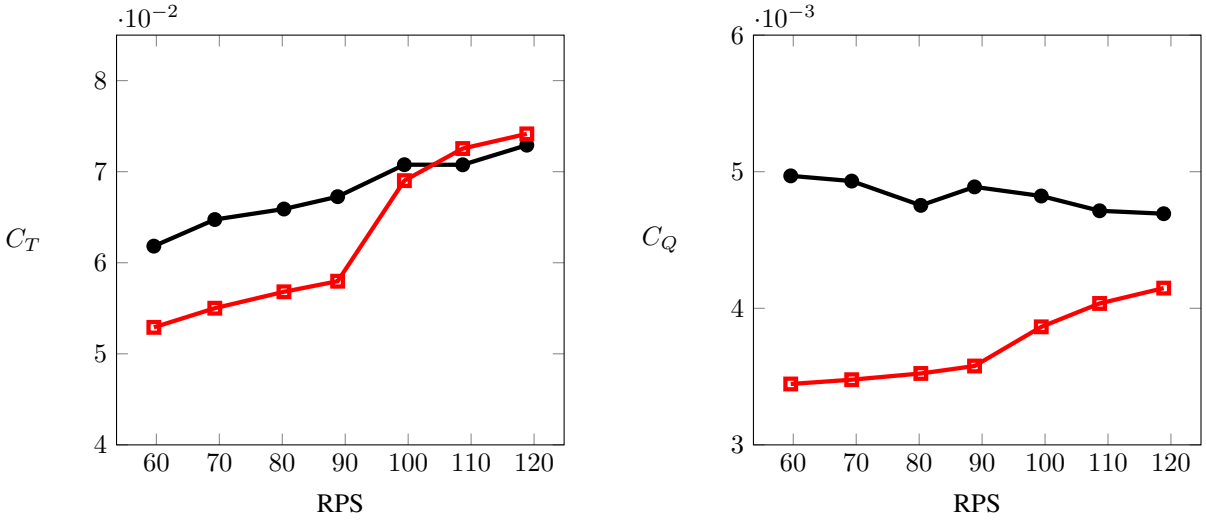

(a) Thrust Coefficient (b) Torque Coefficient

Figure 6: Experimental **??** and numerical **??** results.

3.2 Noise

In the acoustic comparisons, Figure 7 displays the comparison between the experimental spectrum signal and the numerical one for a microphone positioned orthogonally to the propeller's rotation axis. The comparison is displayed for the two rotations limits - 60 and 120 RPS-, as they represent the other rotations' behavior. For the first BPF, results show great similarity, for higher BPFs the spectrum commences to deviate, the phenomena are more evident in higher rotational speed, as well-defined higher BPF are more likely to appear in higher speeds. As a result of the spectrum integrations, Figure 8 unveils the OASPL comparison for rotations. For 60 RPS it is observed the higher deviation, which is close to 3 dB. On the other hand, for the next rotations, the average deviation drops to 2,4 dB with corresponding tendencies between experimental and numerical data.

Hence, Figure 9, exhibits the first BPF directivity level extracted from the spectrum for the experimental and the numerical predictions for then microphones displayed in a polar arc with angles measured from the propeller rotation axis. The level in SPL uses the same band as in the experimental data (5 Hz). The higher deviations are no more than 5 dB and the average deviation is close to 2.5 dB. It is observed also a good correlation between the two data regarding a cardioid pattern.

To assay the broadband, Figure 10 dispose of the spectrum in third-octave bands. The comparison between experiments shows high tendency capture, especially in low rotation speeds. In contrast, the rotational speed increment implicates in small peaks of the energy, which are not captured for the numerical prediction.

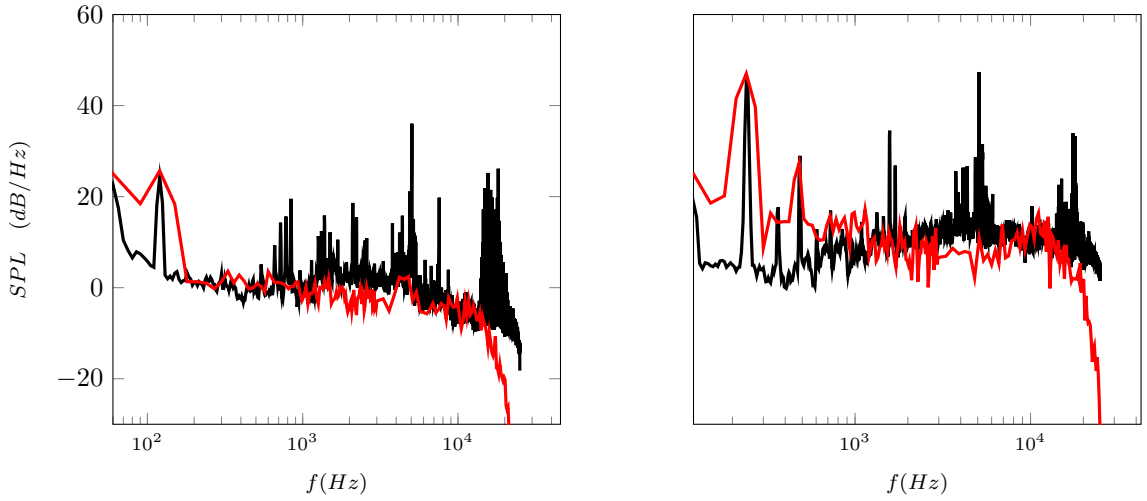

(a) 60 RPS (b) 120 RPS

Figure 7: Experimental **??** and numerical **??** results.

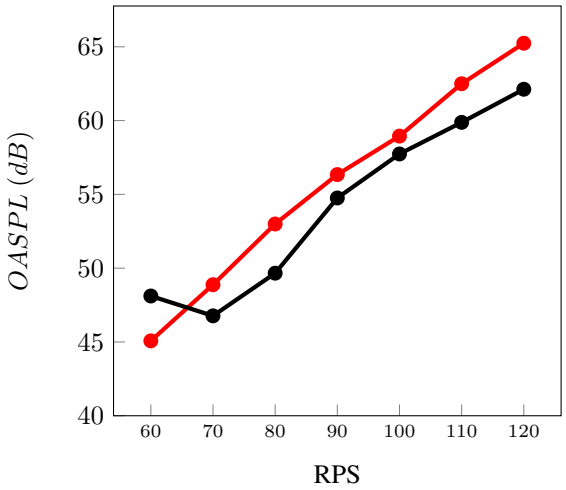

Figure 8: Experimental **??** and numerical **??** results.

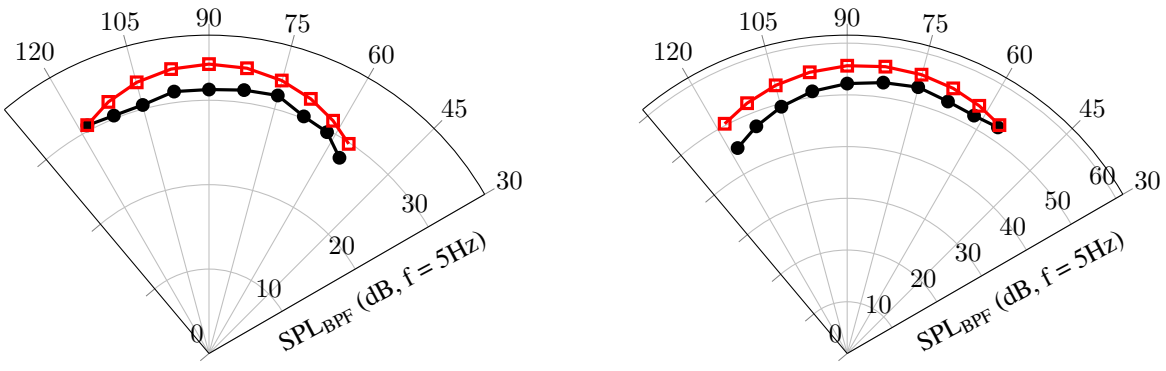

(a) 60 rps (b) 120 rps

Figure 9: Experimental **??** and numerical **??** results.

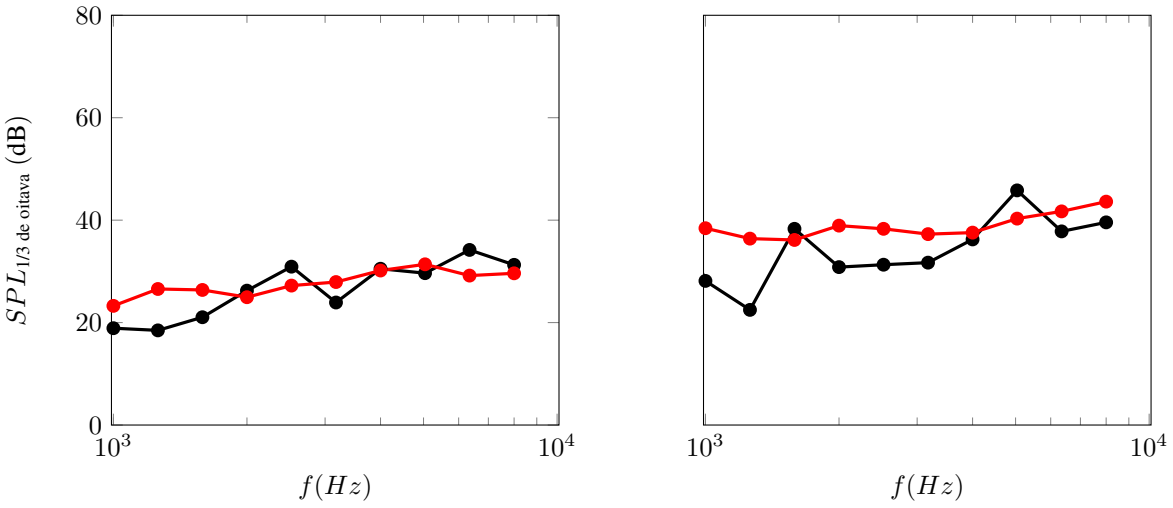

(a) 60 RPS (b) 120 RPS

Figure 10: Experimental **??** and numerical **??** results.

4. CONCLUSIONS

In the light of the novel electric airplane designs using propellers and their possible use in the urban areas, the prediction of the aerodynamics and acoustics behavior of a propeller impose major difficulties arising from the complex nature of the flow. Those difficulties are even more severe in the high frequencies of broadband noise. Numerical simulations based on the Navier-Stokes equations show promising results, but at a high computational cost. Conversely, lattice-Boltzmann-based LES simulations can deliver highly accurate results with much less computational costs than classical LES approaches.

The evaluation of this performance against experimental data displays good accuracy. For the aerodynamic performance, even the highest error is no greater than other numerical approaches and for higher rotational speeds the deviations are much less than other numerical approaches. For the acoustic prediction, which is the most challenging one, the prediction of OASPL and tonal BPF noise levels are, respectively, 2,4 dB and close to 2 dB. This result is more accurate than other numerical techniques. Moreover, very promising results are displayed for the broadband noise in high frequencies using the third-octave bands.

It can be concluded that the lattice-Boltzmann-based LES is a promising technique for this type of prediction. However, limitations in the turbulence model require more considerations, their solution will further improve the results.

5. ACKNOWLEDGEMNT

This paper was possible due to the financial and technical support of EMBRAER and its engineers, specially: Alysson Kenerlly Colacitti, Eduardo Lobão Capucho Coelho and Leandro Guilherme Crenite Simões. Also the financial aid of the Santa Catarina's Teaching and Engineering Foundation – FEESC.

6. REFERENCES

Airway, 2020. "Anac autoriza teste para entrega de produtos com drones". https://www.airway.com.br/embraer-divulga-imagens-de-seu-primeiro-aviao-eletrico/.

Amiet, R.K., 1976. "Noise due to turbulent flow past a trailing edge". Journal of Sound and Vibration 47 (3) (1976) 387–393.

Avallone, F., Casalino, D. and Ragni, D., 2018. "Impingement of a propeller-slipstream on a leading edge with a flow-permeable insert: A computational aeroacoustic study".International Journal of Aeroacoustics, Vol. 17, pp. 687–711.

Avallone, F., Van Den Ende, L., Li, Q., Ragni, D., Casalino, D., Eitelberg, G. and Veldhuis, L., 2019. "Aerodynamic andaeroacoustic effects of swirl recovery vanes length".Journal of Aircraft, Vol. 56, No. 6, pp. 2223–2235.

Bhatnagar, P.L., Gross, E.P. and Krook, M., 1954. "A model for collision processes in gases. i. small amplitude processesin charged and neutral one-component systems".Phys. Rev., Vol. 94, pp. 511–525.

Castilho, R., 2020. "Que tal dar uma voltinha no uber voador desenvolvido pela embraer?" https://www.melhoresdestinos.com.br/embraer-carro-voador.html.

Dassault Systèmes Simulia, 2020, Corp PowerFLOW 6-2019 USER'S GUIDE. Versailles, France. Accessed 12 December 2020.

Ffowcs Williams, J.E., Hawkings, D.L. and Lighthill, M.J., 1969 “Sound generation by turbulence and surfaces in arbitrary motion”.Philosophical Transactions of the Royal Society of London. Series A, Mathematical and Physical Science

Gonzalez-Martino, I., Romani, G., Wang, J. and Casalino, D., 2018 “Rotor noise generation in a turbulent wake using lattice-boltzmann methods”. IAA/CEAS Aeroacoustics Conference.

HKUST, 2020, Experimental data, Hong Kong University of Technology, Hong kong, China, https://aantc.ust.hk. Accessed 12 December 2020.

Ingraham, D., Gray, J. and Lopes, L.V., 2019 “Gradient-based propeller optimization with acoustic constraints”. AIAA Scitech Forum.

Ol, M., Zeune, C. and Logan, M., 2008. “Analytical - Experimental comparison for small electric unmanned air vehicle propellers”. Collection of Technical Papers - AIAA Applied Aerodynamics Conference. August. doi:10.2514/6.2008-7345

KRÜGER, T.; KUSUMAATMAJA, H.; KUZMIN, A.; SHARDT, O.; SILVA, G.; VIGGEN, E.M. The lattice Boltzmann Method: Principles and Practice: Springer International Publishing, 2016. (Graduate Texts in Physics).

Leng, Y., Yoo, H., Jardin, T., Bronz, M. and Moschetta, J.M., 2019 “Aerodynamic modelling of propeller forces and moments at high angle of incidence”.

Lighthill, M.J. and Newman, M.H.A., 1951. “On sound generated aerodynamically i. general theory”.Proceedings of the Royal Society of London. Series A. Mathematical and Physical Sciences, Vol. 211, No. 1107, pp. 564–587.

Rohacs, J. and Rohacs, D., 2019. “Conceptual design method adapted to electric/hybrid aircraft developments”.International Journal of Sustainable Aviation, Vol. 5, No. 3.

Smith, M., 2004.Aircraft Noise. Cambridge University Press

Strash, D.J., Lednicer, D.A. and Rubin, T.D., 2008“Analysis of propeller-induced aerodynamic effects”. Applied Aerodynamics Conference.

SUCCI, S. The lattice Boltzmann Equation: For Complex States of Flowing Matter: Oxford University Press, 2018.

Viswanathan, V. and Knapp, B.M., 2019. “Potential for electric aircraft”. Nature Sustainability, Vol. 2, No. 2, pp. 88–89.

Welch, P., 1967. “The Use of Fast Fourier Transform for the Estimation of Power Spectra: A Method Based on Time Averaging Over Short, Modified Periodograms”. IEEE Transactions on Audio and Electroacoustics, 15, 70-73.

ZHU, Tao; CAROLUS, Thomas. Axial fan tip clearance noise: Experiments,lattice– Boltzmann simulation, and mitigation measures. International Journal of Aeroacoustics, v. 17, p. 159–183, 2017.

7. RESPONSIBILITY NOTICE

The following text, properly adapted to the number of authors, must be included in the last section of the paper:
The author(s) is (are) solely responsible for the printed material included in this paper.